JPNT 9(3), 191-205 (2020)
https://doi.org/10.11003/JPNT.2020.9.3.191

JPNT Journal of Positioning, Navigation, and Timing

Investigation on Figures-of-Merit of Signal Performance for Next Generation RNSS Signal Design

Kahee Han[1], Jong-Hoon Won[2†]

[1]Autonomous Navigation Lab., Inha University, Incheon 22212, Korea
[2]Department of Electrical Engineering, Inha University, Incheon 22212, Korea

ABSTRACT

Designing a new signal is essential in the development of a new Radio Navigation Satellite Service (RNSS) system. This paper introduces the signal design parameters and the figures of merit (FoMs) to be considered in designing a new RNSS signal, and then reviews their relationship in details. In addition, we show examples of the trade-off analysis between FoMs according to the signal design scenarios using an analytical simulation tool based on the relationship between the signal design parameters and the FoMs.

Keywords: RNSS, GNSS, figure of merit, signal design parameters, analytical simulation

1. INTRODUCTION

A Radio Navigation Satellite Service (RNSS) is a Radio Determination Satellite Service used for the purpose of radio navigation including Global Navigation Satellite Service (GNSS) (ITU 2016a). As Position, Navigation, and Timing (PNT) services have become a critical and essential component of national infrastructure and civil and commercial applications, the RNSS system is becoming increasingly important to modern society. According to Esper et al. (2020), the U.S. Global Positioning System (GPS) is a cornerstone of the national PNT architecture, and the GPS modernization effort are underway to improve positioning and timing accuracy, availability, and integrity monitoring support capability. The other space powers such as Russia, Europe, China, Japan, and India recognize the importance of the RNSS system and are steadily working on building their own RNSS systems or modernizing existing systems. Recently, South Korea also begins internally to discuss on a development plan for its own RNSS system, so called Korean Positioning System (KPS), with the goal of 2035 (Park & Heo 2019), and the signal design team began its operation earlier in 2018.

Designing a new RNSS signal is essential in developing a new RNSS system or modernizing the existing system. The RNSS space powers are using their own RNSS signals and steadily working on designing new signals for a better performances as a part of system modernization. There are many challenges in the RNSS signal design, such as signal performance improvements versus resource limitations, compatibility and interoperability between the existing RNSS signals, and trade-offs between various signal performances. In addition, the signal performances are determined by the channel and the receiver resources as well as the signal design parameters, so we have to take into account the receiving environment and the RNSS receiver specifications. However, it is impossible to consider these challenges using real measurements of signals in space from the satellites at the initial signal design phase.

For this reason, we suggest to use the RNSS signal design simulation tool in order to evaluate the designed RNSS signal performance, and to analyze the trade-offs between signal performances. To implement the RNSS signal design

Received Jul 28, 2020 **Revised** Jul 29, 2020 **Accepted** Jul 31, 2020
†**Corresponding Author**
E-mail: jh.won@inha.ac.kr
Tel: +82-32-860-7406 Fax: +82-32-863-5822
Kahee Han https://orcid.org/0000-0001-8804-5120
Jong-Hoon Won https://orcid.org/0000-0001-5258-574X

simulation tool, we need to select appropriate figures-of-merit (FoMs) to represent the signal performance quantitatively and investigate the relationship between the signal design parameters and the FoMs. Therefore, this paper reviews the basic concept of the RNSS signal and the FoMs according to the RNSS signal transmission/reception chain and shows examples of trade-off analysis using the simulation tool.

The remainder of this paper is organized as follows. Section 2 briefly describes the basic concept of the RNSS signal. In Section 3, we review the FoMs according to each part of the RNSS signal transmission/reception chain and describe the relationship between the signal design parameters and each FoM. Section 4 presents examples of the trade-off analysis between FoMs using the developed RNSS signal design simulation tool with several scenarios. Finally, we conclude the paper in Section 5 by outlining the trade-off analysis results.

2. RNSS SIGNALS

The transmitted RF RNSS signal can be represented using complex envelope notation as follows:

$$s(t) = \Re\{x(t)e^{j2\pi f_c t}\} \tag{1}$$

where $s(t)$ is a real-valued RF signal, $x(t)$ is the complex envelope (also called complex baseband signal) of the RF signal, and f_c is the carrier frequency.

The complex envelope contains information to be transmitted and can be expressed in complex forms as follows:

$$\begin{aligned} x(t) &= A(t)e^{j\phi(t)} \\ &= x_I(t) + jx_Q(t) \end{aligned} \tag{2}$$

where $A(t)$ and $\phi(t)$ is the magnitude and the phase of the complex envelope, respectively. It is noted here that the subscripts I and Q represent in-phase and quadrature components, so that and $x_I(t)$ and $x_Q(t)$ are the in-phase and quadrature components of the complex envelope, respectively.

The RNSS signals are generated using the direct sequence spread spectrum technique except for conventional GLONASS signals. Therefore, the RNSS signal can be obtained by modulating the data bit sequence, i.e., the navigation message bits, with the spreading code. The spreading code is also called pseudo-random noise (PRN) code transforming the data bit sequence to a noise-like signal. Using the signal transmission power, data bit sequence, and spreading code, we can rewrite the complex envelope in Eq. (2) as follows.

$$\begin{aligned} x(t) = \sqrt{\gamma_I P_T} \sum_{k=-\infty}^{\infty} \sum_{l=-\infty}^{\infty} c_{I,l} d_{I,k} p_{T_{d,I}}(t - kT_{d,I}) g_I(t - lT_{c,I}) \\ + j\sqrt{\gamma_Q P_T} \sum_{\infty}^{\infty} \sum_{\infty}^{\infty} c_{Q,n} d_{Q,m} p_{T_{d,Q}}(t - kT_{d,Q}) g_Q(t - lT_{c,Q}) \end{aligned} \tag{3}$$

where, P_T is the total transmit power of the complex envelope, γ_I and γ_Q are power split coefficients between in-phase and quadrature component (i.e. $\gamma_I+\gamma_Q=2$ and γ_I, $\gamma_Q \geq 0$), $T_{d,I}$ and $T_{d,Q}$ are the data bit duration, $T_{c,I}$ and $T_{c,Q}$ are the spreading code chip duration, $\{c_{I,l}\}$ and $\{c_{Q,n}\}$ are the spreading codes with $c_{I,l} \in \{-1,+1\}$ and $c_{Q,n} \in \{-1,+1\}$, $\{d_{I,k}\}$ and $\{d_{Q,m}\}$ are the data bit sequences with $d_{I,k} \in \{-1,+1\}$ and $d_{Q,m} \in \{-1,+1\}$, $p_{T_{d,I}}(t)$ and $p_{T_{d,Q}}(t)$ are waveform generation functions for the data bit sequence, and $g_I(t)$ and $g_Q(t)$ are waveform generation functions for the spreading code of the in-phase and the quadrature component.

Most of RNSS signal uses the phase shift keying (PSK) modulation with a rectangular shape of pulse (non-return to zeros), so we can define waveform generation functions in Eq. (3) as follows.

$$\begin{aligned} p_{T_d}(t) &\triangleq \begin{cases} 1, & 0 \leq t \leq T_d \\ 0, & otherwise \end{cases} \\ g(t) &\triangleq \begin{cases} 1, & 0 \leq t \leq T_d \\ 0, & otherwise \end{cases} \end{aligned} \tag{4}$$

Meanwhile, some of the modernized RNSS signals use the binary offset carrier (BOC) modulation to minimize spectral overlap with the existing RNSS signals. The BOC signal can be generated by multiplying the subcarrier with the BPSK signal. In general, we use a sequence of a sign of sinusoidal with a frequency f_s as a subcarrier. Therefore, the subcarrier can be expressed as follows.

$$\begin{aligned} &sign[\sin(2\pi f_s t)] && (\text{for BOC}_{\sin}) \\ &sign[\cos(2\pi f_s t)] && (\text{for BOC}_{\cos}) \end{aligned} \tag{5}$$

As shown in Eqs. (1-5), the RNSS signal basically consists of the carrier, the spreading code, and the navigation data. Therefore, the characteristics of the RNSS signal are determined according to how to set the parameters for each component. For example, we have to make a decision on which data rate and message structure we will use as to the navigation message. Fig. 1 shows the RNSS signal design parameters for each component.

3. FIGURES OF MERIT

When we design a new RNSS signal, we must consider the system-level accuracy requirements. The system-

https://doi.org/10.11003/JPNT.2020.9.3.191

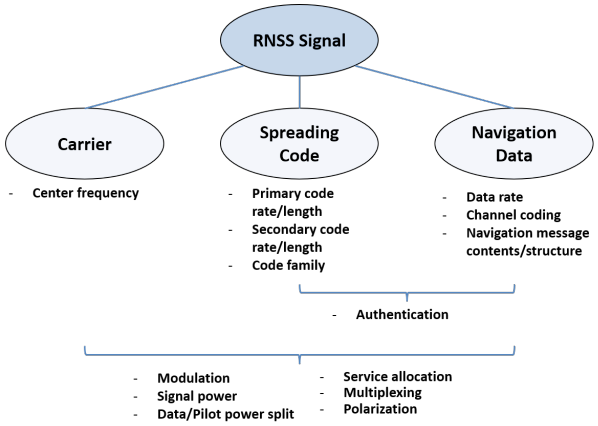

Fig. 1. RNSS signal design parameters (Han & Won 2018).

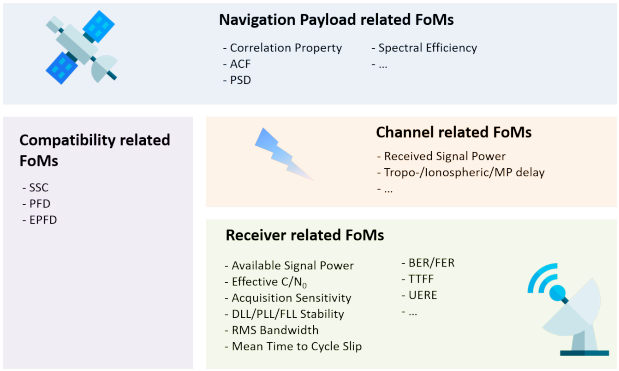

Fig. 2. Figures of merit in signal transmission/reception chain (Han & Won 2018).

level accuracy requirements can be translated into signal measurement accuracy requirements, such as pseudorange accuracy. In addition to this, the RNSS signal should have the following properties (Spilker 1996a):

- Multiple access capability
- Robustness to some level of multipath interference
- Anti-jamming and anti-spoofing capability

The RNSS signal performance, which indicates how good the signal measurement quality and the signal properties are, can be quantified using various FoMs. Meanwhile, the signal performance depends not only on the signal characteristics but also on the satellite navigation payload as well as the receiver hardware and how to process the signal in the receiver. In this paper, we focus on the FoMs, which are mainly determined by the signal characteristics. The FoMs can be categorized by the related part of the RNSS signal transmission/reception chain as shown in Fig. 2.

3.1 Navigation Payload Related FoMs

The RNSS signal is generated and transmitted by the navigation payload. The payload of the navigation satellite is basically composed of a clock unit, a navigation signal generation unit, a frequency generation and modulation unit, a high power amplifier (HPA), a output multiplexer, and an antenna (Rebeyrol et al. 2006). The following subsection covers the FoMs related to the navigation payload.

3.1.1 Correlation property

Each satellite is identified by the allocated PRN code. In ideal case, the PRN code needs to have orthogonality with any other PRN code in the same family. Also, the PRN code should have to be distinguishable from its time-shifted version. According to Wallner et al. (2011), these requirements can be checked by calculating the correlation percentile. The lower correlation value at the same percentile, except for 100 percent (i.e. the autocorrelation value with itself), means that this PRN code family has a better correlation property than others.

Related signal design parameters: PRN code family, code length

3.1.2 Autocorrelation function

In the acquisition process, we use the ambiguity function, which is a two-dimensional function of the code delay and the Doppler frequency, to determine whether the desired signal exists. Assuming a zero Doppler frequency , the ambiguity function is equal to the correlation function in the code delay domain. The correlation function is performed on the received RNSS signal and the local replica, so the output of the correlation function is dominantly affected by the adopted modulation method.

The shape of the autocorrelation function is related to its acquisition and tracking complexity and ranging error performance (Fine & Wilson 1999, Betz 1999). The autocorrelation function of the BPSK signal has very small side lobe peaks with respect to the main lobe peak, but the BOC signal has non-negligible side lobe peaks. These non-negligible side lobe peaks may cause false detection in a noisy environment, and the false detection causes tracking and reacquisition meaningless, so they need a longer integration time to compensate the noise effect. To reduce false detection, the difference between the main lobe and side lobe peaks of the autocorrelation function should be large. Also, the non-negligible side lobe peaks cause multiple zero-crossing points in the delay lock loop

(DLL) discriminator output, which may cause a false lock. Therefore, the shape of the autocorrelation function and the ratio of the autocorrelation main lobe peak with respect to the biggest sidelobe peak can be used to evaluate the signal performance (Won et al. 2011).

Related signal design parameters: PRN code family, chipping rate, modulation

3.1.3 Power spectral density

One of the main characteristics of the RNSS signal is the power spectral density (PSD) that can be obtained by the Fourier transform of the autocorrelation function. The PSD indicates how the signal power is distributed in the frequency domain. The shape of the PSD directly affects tracking accuracy, multipath mitigation performance, and compatibility with other RNSS signals (Xue et al. 2015). The PSD with the large main lobe width has good tracking accuracy and multipath mitigation performance but may be widely overlapped with other RNSS signals in the same band, which induces a poor compatibility of the signal. On the other hand, the signal with a wide main lobe or separated two main lobes requires a wide front-end bandwidth, which inevitably increases the receiver implementation cost. That is, the signal should be designed to have a PSD suitable for the purpose of the signal.

Related signal design parameters: chipping rate, modulation, transmit power

3.1.4 Spectral efficiency

The RNSS signal is transmitted at the antenna through the HPA of the satellite payload, and various problems are introduced by the distortion caused by the nonlinearity of the HPA, and the out-of-band emission (OOBE) may be a critical problem depending on the frequency band. According to ITU (2015), the OOBE is the emission on a frequency or frequencies immediately outside the necessary bandwidth which is resulted by the modulation process. The RNSS signals share the same frequency band or adjacent band with other systems. Therefore, a strict restriction on the OOBE of the RNSS signals is required based on the following facts for the compatibility with other signals (Xue et al. 2015):

- signals with relatively low OOBE power significantly mitigate signal distortion due to non-ideal filter characteristics, and
- signals with relatively low OOBE power have low noise levels that meet stringent constraints. It also contributes to reducing the complexity and cost of designing satellite filters.

Meanwhile, the energy efficiency of the satellite is a key consideration because of their finite power source. Therefore, to minimize power loss caused by OOBE, a proper modulation method should be selected in consideration of the necessary frequency bandwidth. The power loss due to OOBE can be quantified by calculating the spectral efficiency η:

$$\eta = \int_{-B/2}^{B/2} G_s(f)df \tag{6}$$

where B is the necessary frequency bandwidth (or receiver front end bandwidth in terms of the RNSS receiver), and $G_s(f)$ is the normalized PSD.

Low spectral efficiency means that the power of the signal is distributed in the out-of-band region. Therefore, in signal design, spectral efficiency must be maximized to efficiently use the frequency resource and ensure compatibility with other services in the adjacent band.

Related signal design parameters: center frequency, chipping rate, modulation

3.2 Channel Related FoMs

In this part, we introduce the FoMs related to the transmission channel.

3.2.1 User received power

The RNSS signal transmitted from the satellite suffers from power loss due to the long transmission distance, the antenna polarization mismatch, the antenna de-pointing, and the atmospheric effects by the ionosphere and the troposphere. Considering these loss factors, the received power at the user receiver antenna can be calculated as follows:

$$\begin{aligned} P_R = {} & 10\log_{10}(P_T G_T G_R) - 10\log_{10}(L_{FSL}) - 10\log_{10} L_T \\ & - 10\log_{10} L_I - 10\log_{10} L_P - 10\log_{10} L_D \end{aligned} \tag{7}$$

where P_T is the transmitted power, G_T is the transmit antenna gain, G_R is the receiver antenna gain, L_{FSL} is the free space loss, L_T is the loss due to the troposphere, L_I is the loss due to the ionosphere, L_P is the polarization mismatch loss, and L_D is the antenna de-pointing loss.

https://doi.org/10.11003/JPNT.2020.9.3.191

The RNSS signals are vulnerable to the RF interference due to their weak signal power. Also, if the received signal power is too weak, the receiver has a poor positioning accuracy. Therefore, in order to have a good robustness against the RF interference and high positioning accuracy, the RNSS signal must be designed to have high enough user received power in the same transmission channel.

Related signal design parameters: center frequency, transmit power, polarization

3.2.2 Tropospheric error

The lowest layer of the Earth's atmosphere, called the troposphere, consists of dry gas and water vapor. The RNSS signals are delayed by refraction by them, and the degree depends on the refraction index n of the atmosphere in the signal transmission path. The signal delays due to troposphere can be divided into drying delays due to dry air and wet delays due to water vapor. Wet delay and dry delay can be obtained by multiplying the mapping function (or obliquity factor) and the zenith delay. The total tropospheric delay can be obtained as shown in Eq. (8) and the detailed process for calculating it is explained in Spilker (1996b).

$$\Delta T = M_d(E)10^{-6}\int N_d ds + M_w(E)10^{-6}\int N_w ds \quad (8)$$

where subscripts d and w refers to the dry and wet term, respectively, $M(E)$ is the mapping function with respect to the elevation angle, and N is the refractivity.

In the frequency band where navigation signals exist, since the troposphere is a non-dispersive medium, the refractivity is constant regardless of frequency and causes the same delay for code and phase. That is, the tropospheric delay has no dependency on the RNSS signal design parameters but the atmospheric condition of the transmission channel and the constellation of the satellites of the system.

Related signal design parameters: None

3.2.3 Ionospheric error

Unlike the troposphere, the ionosphere is a dispersive medium at several GHz. Therefore, the ionosphere has a different refractive index depending on the frequency. The ionospheric refractive index is determined by the carrier frequency and the polarization of the RNSS signal, and the process of calculating it is detailed in Hoque & Jakowski (2012). According to Klobuchar (1996), the ionospheric refractive index can be expressed simply as a function of $1/f^2$ and the total ionosphere delay considering the slant distance using the mapping function can be written as follows:

$$\Delta I = -\frac{40.3}{f^2}TEC \cdot M(E) \quad (9)$$

where f is the carrier frequency, TEC is the total electron content.

Related signal design parameters: center frequency, polarization

3.2.4 Multipath error

The multipath refers to a phenomenon in which the desired signal is reflected or diffracted to reach a receiver through two or more paths. The effects of the multipath depend on the amplitude, the delay, the phase, and the rate of change of the phase of the reflected signal with respect to the direct signal. The multipath signals can distort the correlation function of the direct signal, therefore the distorted discriminator output induces the pseudorange error. From this, we know that if the correlation function of the multipath is separated enough from the correlation function of the direct signal, there is no pseudorange error caused by the multipath. According to Misra & Enge (2012), if the multipath delay is greater than $T_c(1+\frac{d}{2})$, where T_c is the chip width in meters and d is the correlator spacing in chips, there is no distortion of the discriminator output and pseudorange error caused by the multipath. The pseudorange error $E(\tau_{MP})$ caused by the multipath can be calculated as follows.

$$E(\tau_{MP}) \approx Disc_{comp}(\tau_{MP}) \cdot T_c \quad (10)$$

where τ_{MP} is the multipath delay and $Disc_{comp}$ is the discriminator output from a composite correlation function $R_{comp}(\cdot)$. The composite correlation function is expressed as follows (Ward & Betz 2006b):

$$R_{comp}(\tau-\tau_0) = R(\tau-\tau_0) + \alpha R(\tau-\tau_0-\tau_{MP})\cdot\cos(\Delta\psi) \quad (11)$$

where τ_0 is the code delay of the direct signal, τ_{MP} is the multipath delay, α is the multipath to direct signal ratio (MDR), and $\Delta\psi$ is the relative phase difference between the direct signal and the multipath.

Related signal design parameters: chipping rate, modulation

3.3 Receiver Related FoMs

The received analog RF RNSS signal is converted to

a digital IF signal through the front end of the receiver. The digital IF signal is used for the signal acquisition, the signal tracking, and the data demodulation, and finally the processing results are used to calculate the receiver's position. Therefore, it is required to analyze signal performance considering the front end and digital signal processing of the receiver.

3.3.1 Available signal power

The received RNSS signal at the receiving antenna on the surface of the Earth has a high frequency and a weak signal power. In addition, analog components are sensitive to the operating environment, so the RNSS receiver uses the front end to condition the incoming analog signal for digital signal processing (Misra & Enge 2012). The signal conditioning chain at the front end consists of filters, amplifiers, and an analog-to-digital converter (ADC), which induces a power loss called implementation loss in the received signal due to band-limiting, sampling, and quantization. The available signal power P_{avail}, that is the signal power at the ADC output, can be calculated as follows:

$$P_{avail} = P_R - 10\log_{10} L_{BSQ} \tag{12}$$

where P_R is the received signal power at the receiving antenna input and L_{BSQ} is the implementation loss due to the signal conditioning at the front end. The implementation loss can be calculated using the analytical model as described in Hegarty (2011).

It is noted here that the transmitted signal power at the satellite payload antenna should be designed to be high enough to provide the required received signal power at ground users even though the power attenuation in the channel.

Related signal design parameters: center frequency, chipping rate, modulation, transmit power, polarization

3.3.2 Effective C/N_0

In terms of the signal processing at the receiver, the quality of the received RNSS signal can be evaluated by the carrier power-to-noise density ratio (C/N_0). Note that the signal used for the signal acquisition, the signal tracking, and the data demodulation is the digital IF signal conditioned by the front end. Therefore, the available signal power should be considered as the carrier power. Besides the aforementioned factors of signal power attenuation, the interference also causes C/N_0 degradation. The effective C/N_0 can be obtained by modeling the interference as the white noise as expressed in the following (Betz 2001):

$$effective\ C/N_0 = \frac{C_s}{N_0 + C_I \dfrac{\int_{-B_r/2}^{B_r/2} G_s(f)G_i(f)df}{\int_{-B_r/2}^{B_r/2} G_s(f)df}} \tag{13}$$

where C_s is the desired signal power, C_I is the interference power, N_0 is the thermal noise density, B_r is the receiver front end bandwidth, $G_s(f)$ is the normalized PSD of the desired signal, and $G_I(f)$ is the normalized PSD of the interference. Note that the remainder of this paper, the C/N_0 means the effective C/N_0.

Related signal design parameters: center frequency, chipping rate, modulation, transmit power, polarization

3.3.3 Acquisition sensitivity

As mentioned earlier, the RNSS signal is very weak, so the signal detection is very difficult in poor environments with many obstacles and interference. Therefore, the capability to detect RNSS signals in harsh environments is important to improve availability of the system. To quantify this capability, we can use an acquisition sensitivity. The acquisition sensitivity is defined as the minimum required signal power to acquire the signal while satisfying the predefined detection probability and false alarm probability (Weill & Petovello 2011). Lower acquisition sensitivity means that signal acquisition is possible even in poor environments. The acquisition sensitivity can be calculated using the dwell time, the detection probability and the false alarm probability (Liu et al. 2010). The dwell time is a function of the coherent integration time and the noncoherent summations. According to Foucras et al. (2014), reducing the number of noncoherent summations and increasing the coherent integration time over a given dwell time improves the acquisition sensitivity. However, the coherent integration time cannot exceed the navigation data bit duration in normal receiver operation.

Related signal design parameters: code length, chipping rate

3.3.4 Delay-/phase-/frequency lock loop stability

According to Won et al. (2008), the tracking loop stability can be analyzed using a minimum required C/N_0 to track a signal, accuracy, dynamic sensitivity, stable region, design margin in terms of noise jitter, and design margin in terms of C/N_0. These key factors are read from a tracking loop's

https://doi.org/10.11003/JPNT.2020.9.3.191

noise jitter plot with a noise jitter threshold. The tracking loop is composed of the DLL, the phase lock loop (PLL), and the frequency lock loop (FLL), and each loop has its own noise jitter characteristics. In case of the DLL, the noise jitter threshold is determined by the correlator spacing and the total noise jitter is determined by the thermal noise jitter and the dynamic stress error. In the PLL, the noise jitter threshold is determined by the discriminator function and the total noise jitter is determined by the thermal noise jitter, the dynamic stress error, the Allan deviation oscillator phase noise, and the vibration induced phase noise. In the FLL, the noise jitter threshold is determined by the coherent integration time and the total noise jitter is determined by the thermal noise jitter, the dynamic stress error, and the Allan deviation oscillator phase noise. A detailed description of the process of calculating the noise jitter threshold and the total noise jitter in each loop is given in Ward & Betz (2006a).

Related signal design parameters: center frequency, chipping rate, modulation, transmit power, polarization, data/pilot power split

3.3.5 RMS bandwidth

The thermal noise jitter of the DLL is determined by the receiver's signal processing parameters, such as the discriminator function, the loop bandwidth, the coherent integration time, the correlator spacing and so on. Therefore, by defining the Cramer-Rao lower bound (CRLB) of the thermal noise jitter, code tracking performance can be evaluated independently of these receiver parameters. Assume that the correlator spacing becomes vanishingly small, the CRLB can be expressed as follows (Xue et al. 2015):

$$\sigma_{tDLL,CRLB} = \sqrt{\frac{B_L}{(2\pi)^2 C/N_0 \int_{-B_r/2}^{B_r/2} f^2 G_s(f) df}} \tag{14}$$

where B_L is the code tracking loop bandwidth and $G_s(f)$ is the normalized PSD of the desired signal.

However, the CRLB in Eq. (14) still depends on the strength of the received signal and the tracking loop bandwidth. Therefore, the code tracking performance can be evaluated independently of the receiving environment and the receiver signal processing setting by using the integral term of the denominator of Eq. (14). The integral term is referred as the root-mean-squared (RMS) bandwidth or Gabor bandwidth and can be expressed as follows.

$$f_{rms} = \sqrt{\int_{-B_r/2}^{B_r/2} f^2 G_s(f) df} \tag{15}$$

According to Ward & Betz (2006a), the RMS bandwidth is a measure of the sharpness of the correlation peak. It is noted that BOC signals has larger RMS bandwidths than PSK signals within the same bandwidth. Intuitively, the greater the RMS bandwidth, the better the code tracking performance.

Related signal design parameters: chipping rate, modulation

3.3.6 Mean time to cycle slip

If the PLL loses lock, the carrier phase observations show discontinuity near at that time. This discontinuity is called cycle slip, and when a cycle slip occurs, the integer ambiguity must be re-determined. The cycle slip is caused by temporary signal shielding due to trees, buildings, and overpasses, ionospheric disturbances, multipath errors, and low signal-to-noise ratio (SNR) due to the low elevation angle. The mean time to cycle slip is a important FoM for evaluating the PLL performance of the RNSS receiver (Won et al. 2008). The mean time to cycle slip can be modeled as follows depending on the order and type of the PLL (Holmes & Raghavan 2009, Liu et al. 2010).

$$\bar{T}_{CS,D} = \frac{\pi}{4B_L} e^{\frac{\gamma}{2\sigma^2_{PLL,D}}} \tag{16}$$

$$\bar{T}_{CS,P} = \frac{\pi}{4B_L} e^{\frac{2\gamma}{\sigma^2_{PLL,P}}} \tag{17}$$

where the $\bar{T}_{CS,D}$, $\bar{T}_{CS,P}$, $\sigma_{PLL,D}$, and $\sigma_{PLL,P}$ are the mean time to cycle slip and the thermal noise for the Costas loop and the pure PLL, respectively, B_L is the loop bandwidth, and the γ is an effective SNR loss factor that depends on the order of the PLL. The effective SNR loss factor is 1, 0.891, and 0.794 for a first-, second-, third-order PLL, respectively.

Related signal design parameters: center frequency, chipping rate, modulation, transmit power, polarization, data/pilot power split

3.3.7 Bit/Frame error rate

In general, data demodulation performance is evaluated using the bit error rate (BER) curve with respect to the E_b/N_0. Navigation messages consist of frames composed of data bits of a certain length, so in order to recover the navigation messages, the frame should be free of bit error. Therefore,

when assessing the data demodulation performance of the RNSS signal, we have to focus on the frame error rate (FER). Meanwhile, most of the FoMs of the RNSS signal are evaluated with respect to the C/N_0, so the BER and the FER should be expressed with respect to the C/N_0.

For the uncoded navigation message and the convolutional coded navigation message, the BER can be expressed as follows:

$$BER_{uncoded} = \frac{1}{2} erfc\left(\sqrt{E_b/N_0}\right) = \frac{1}{2}\, erfc\left(\sqrt{\alpha_D \frac{C/N_0}{R_d}}\right) \quad (18)$$

$$BER_{CC} = \frac{1}{2}[36D^{10} + 211D^{12} + 1404D^{14} + 11633D^{16}] \quad (19)$$

with

$$D = e^{\left(-\frac{E_b/N_0}{2}\right)} = e^{\left(-\alpha_D \frac{C/N_0}{2R_d}\right)}$$

where, α_D is the ratio of the signal power on the data component and R_D is the data rate.

The FER can be obtained based on the BER of the corresponding signal and their relationship can be expressed as follows.

$$FER = 1 - (1 - BER)^{N_{frame}} \quad (20)$$

where N_{frame} is the frame length in bits.

Related signal design parameters: center frequency, chipping rate, modulation, data rate, transmit power, polarization, data/pilot power split, navigation message contents/structure

3.3.8 Time-to-first-fix

The time-to-first-fix (TTFF) is a measure of the time that takes to get the first position fix after switching on the receiver. The TTFF is defined as the sum of several time consuming factors. Assume that the receiver status is a cold start, i.e. factory reset mode, the TTFF can be expressed as follows (Anghileri et al. 2008):

$$TTFF = T_{warm-up} + T_{acq} + T_{trk} + T_{CED+GST} + T_{PVT} \quad (21)$$

where $T_{warm\text{-}up}$ is the receiver warm-up time to operate properly, T_{acq} is the time it takes to acquire a signal, T_{Trk} is the time it takes for the tracking loop to enter the stable region, $T_{CED+GST}$ is the time it takes to recover navigation messages (i.e., block correction and ephemeris data (CED) and GNSS system time (GST)) from the data of the received signal, and T_{PVT} is the time to compute the PVT solution usint the CED and the GST.

Among the above time consuming factors, the acquisition time T_{acq} and the data recovery time $T_{CED+GST}$ are dominant components of the TTFF and are determined by the RNSS signal design parameters. The acquisition time is determined by the spreading code length and the possible Doppler frequency range, and the data recovery time is determined by the allocation of the navigation message contents.

Related signal design parameters: center frequency, code length, chipping rate, modulation, data rate, transmit power, polarization, data/pilot power split, navigation message contents/structure

3.3.9 User equivalent range error budget

According to Conley et al. (2006), to analyze the effect of the measurement errors on accuracy, we assume that the error sources can be allocated to individual satellite pseudorange, generating the equivalent error in each pseudorange. The effective accuracy of the pseudorange is termed as the user-equivalent range error (UERE). That is, the UERE is a measure of the pseudorange measurement error for each observed satellite, and it can be used to predict the positioning accuracy of the system. The system UERE is defined as root-sum-square (RSS) of the user range error (URE) and the user equipment error (UEE), which can be expressed as follows (NAVSTAR GPS 1996):

$$\sigma_{UERE} = \sqrt{\sigma_{UEE}^2 + \sigma_{URE}^2} \quad (22)$$

The URE is the error caused by the space and the control segments, such as frequency standard stability, space vehicle acceleration uncertainty, and the ephemeris prediction and model implementation error. The UEE is the error caused by the user segment, such as the ionospheric/tropospheric delay compensation error, receiver noise and resolution, and the multipath. Assuming that each error factor is independent and identically distributed (i.i.d), the UERE can be treated as a Gaussian random variable.

Related signal design parameters: center frequency, chipping rate, modulation, transmit power, polarization, data/pilot power split

3.4 Compatibility Related FoMs

When designing a new RNSS signal, it is necessary to analyze the effect of the interference by the new RNSS signal on existing systems in the same or adjacent bands, and vice

versa. In this part, we introduce the FoMs can be used to analyze the compatibility.

3.4.1 Spectral separation coefficient

The spectral separation coefficient (SSC) is a FoM for quantifying and indicating the performance degradation caused by interference at the correlator output. The SSC can be calculated using the following formula.

$$k_{ls} = \int_{-B_r/2}^{B_r/2} G_i(f) G_s(f) df \tag{23}$$

where B_r is the complex bandwidth of the receiver front-end, and $G_I(f)$ is the normalized PSD of the aggregate interference.

The SSC is used to determine compatibility with existing signals when designing new signals at the first design phase. Each existing RNSS signal has a limit on the tolerable aggregate effective noise level, and the SSC between the existing signal and the new signal can be used to determine whether the aggregate effective noise level exceeds the threshold. When designing a new RNSS signal in the L1 band, it is necessary to consider the SSCs between the new signal and the existing RNSS signals such as L1 C/A code, P(Y) code, L1C, and M code signal. Betz & Goldstein (2002) shows how to calculate the upper bound of the SSCs between the new RNSS signal and existing signals. For example, to ensure compatibility with the C/A code signal, the SSC between the C/A code and the new signal must lower than -76.4 dB-Hz.

Related signal design parameters: chipping rate, modulation

3.4.2 Equivalent power flux density

The RNSS signal reaching the ground act as interference to the receiver in other systems. To protect other RF systems allocated in the same or adjacent band, the RNSS system must comply with the power flux density (PFD) and aggregate equivalent power flux density (EPFD) limits regulated by the ITU. The PFD is the signal power per unit area at the ground and the EPFD is the PFD which takes into account the aggregate of the emissions from all non-geosynchronous orbit (GSO) satellites in the direction of any GSO receiver, taking into account the GSO antenna directivity (Matas 2018). Acceptable interference level, i.e. the PFD or the EPFD limits, can be determined using the PFD when the geometry between the system to be protected and the interferer is fixed, otherwise using EPFD. Since RNSS includes non-GSO, we should check whether the EPFD of the new RNSS system is lower than the acceptable interference level. The EPFD in dBW/MHz is calculated as follows (ITU 2016a):

$$EPFD = 10\log_{10}\left[\sum_{i=1}^{N} 10^{\frac{P_i}{10}} \cdot \frac{G_t(\theta_i)}{4\pi d_i^2} \cdot \frac{G_r(\varphi_i)}{G_{r,max}}\right] \tag{24}$$

where N is the number of visible satellites from the receiver, P_i[dBW] is the transmit power at the input of the antenna of the non-GSO in the reference bandwidth, θ_I is the off-axis angle between the boresignth of the satellite and the direction if the receiver, $G_T(\cdot)$ is the transmit antenna gain of the satellite, d_I is the transmission distance, ϕ_I is the off-axis angle between the pointing direction of the receiver and the direction of the transmit antenna, $G_r(\cdot)$ is the receive antenna gain of the receiver, and $G_{r,max}$ is the maximum gain of the receiver.

For examples, to protect the Aeronautical Radio-Navigation Service in the L5 band, the ITU requires that the EPFD of all RNSS systems in the same band do not exceed –121.5 dBW/m^2 in a 1 MHz. In the C band, to protect Radio Astronomy Service (RAS) operating in the 4990-5000 MHz, the PFD produced by any GSO RNSS and the EPFD produced by all non-GSO RNSS operating in the 5010-5030 MHz should not exceed -171 dBW/m^2 and -245 dBW/m2 in a 10 MHz, respectively (ITU 2016b).

Related signal design parameters: chipping rate, modulation, transmit power

4. TRADE–OFF ANALYSIS BETWEEN FIGURES OF MERIT

The new RNSS signal design is pursued to have a better performance than the existing RNSS signal. However, adjusting the signal design parameters to improve one performance may lead to the other performance degradation. Therefore, we should perform a trade-off analysis between the FoMs at the same time as deriving the signal candidates. The trade-off analysis is based on the complex relationship between the FoMs and the signal design parameters. Using a simulator based on the relationship between the FoMs and the signal design parameters makes it easy to perform such a complex trade-off analysis (Han & Won 2019, Shin et al. 2019). Table 1 is a mapping table for mapping the key signal design parameters related to each FoM. This section performs a trade-off analysis between the FoMs based on the Table 1

Table 1. Signal design parameters vs figures of merit.

Figures of merit	Signal design parameters							
	Center frequency	Chipping rate	Code length	Data rate	Navigation message type	Modulation	Transmit power	Signal power split
Normalized ACF		x				x		
PSD		x				x	x	
Spectral efficiency		x				x		
User received power	x						x	
Ionospheric error	x							
Multipath error		x				x		
Available signal power	x	x					x	
Effective C/N_0	x	x				x	x	
Acquisition sensitivity		x	x					
DLL/PLL/FLL stability	x	x				x	x	x
RMS bandwidth		x				x		
Mean time to cycle slip	x	x				x	x	x
BER	x	x		x		x	x	x
FER	x	x		x	x	x	x	x
TTFF	x	x	x	x	x	x	x	x
UERE budget	x	x		x		x	x	x
SSC		x				x		
PFD/EPFD		x				x	x	

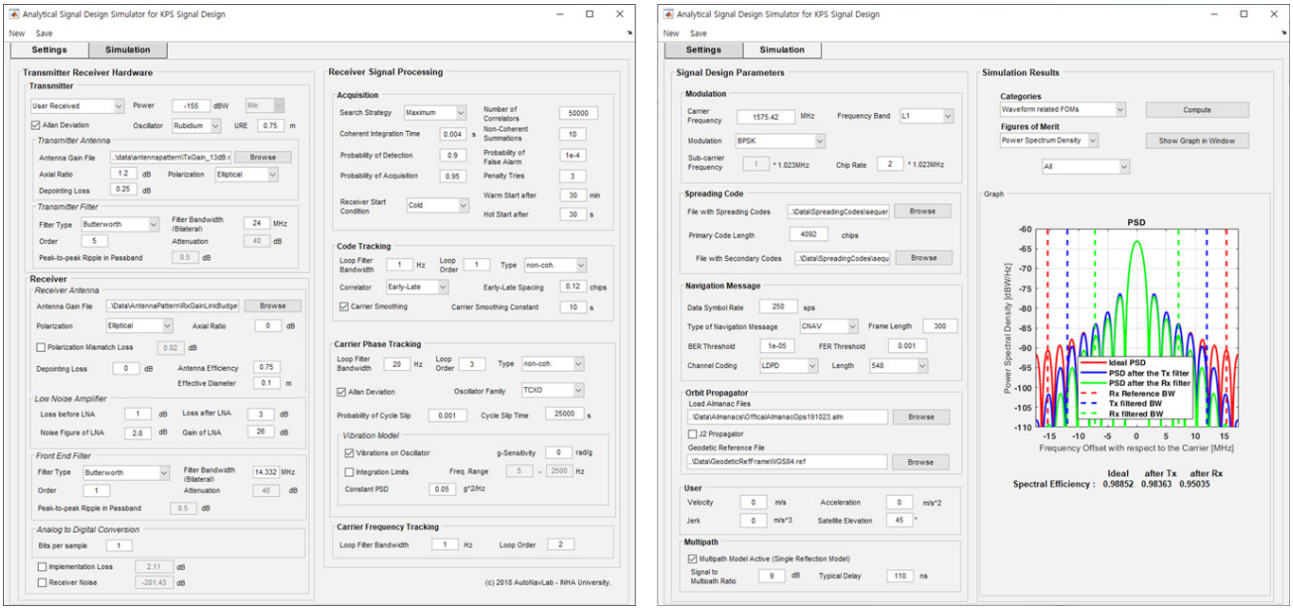

Fig. 3. Settings tab (left) and simulation tab (right) of the GUI of the signal performance verification software (Han & Won 2019).

for an example using the analytical simulator as shown in Fig. 3.

4.1 Spectral Efficiency vs Multipath Error vs RMS Bandwidth

The spectral efficiency, the multipath error, and the RMS bandwidth are related to the chipping rate and the modulation. Based on the relationship between each FoM and the signal design parameter, the higher the PSD value is near the center frequency, the higher the spectral efficiency is obtained. On the other hand, the RMS bandwidth is wider as the PSD value of the high frequency component, that is, the frequency component farther from the center frequency, is higher. Meanwhile, multipath error performance can be evaluated using a multipath error envelope and a minimum value of an acceptable multipath delay as a quantitative index. The ranging error due to multipath is caused by the discriminator output error due to the distorted autocorrelation function. Therefore, the narrower the correlator spacing and the correlation peak of the direct signal are, the more robust to the multipath is obtained.

Table 2 represents simulation parameters having a great influence on these FoMs other than the signal design

parameters. To analyze the trade-offs between the three FoMs according to the chipping rate and the modulation, these simulation parameters are common to all scenarios.

Fig. 4 and Table 3 show the simulation results of the normalized PSD (Fig. 4a), the multipath error envelope (Fig. 4b), and the RMS bandwidth (Fig. 4c) of all scenarios with the parameters as in Table 2. As we can see from Fig. 4a and Table 3, the higher the signal power is concentrated near the center frequency, the higher the spectral efficiency is obtained. For the same chipping rate, the BPSK signal has a better spectral efficiency than the BOC signal, and for the BPSK signal, the lower the chipping rate is, the better. In the case of BOC modulation, the lower the subcarrier frequency is, the closer the two main lobes are to the center frequency, thus having a better spectral efficiency. The $BOC_{cos}(2,1)$ has the worst case in terms of the spectral efficiency among the simulation scenarios. This is because the side lobes near the center frequency are small and the frequency components outside the two main lobes have large sidelobes compared to $BOC_{sin}(2,1)$.

Table 2. Simulation parameters for trade-off analysis – spectral efficiency, multipath error, and RMS bandwidth.

Scenarios	Tx. filter (BW [MHz])	Rx. filter (BW [MHz])	Correlator spacing [chips]	Discriminator type	MDR [dB]
BPSK(1) BPSK(10) $BOC_{sin}(1,1)$ $BOC_{sin}(2,1)$ $BOC_{cos}(2,1)$	Brickwall (150)	1st order butterworth (24)	0.1	Coherent EML	-3

The multipath error envelope shown in Fig. 4b indicates the upper and lower bounds of the multipath error caused by the constructive multipath and destructive multipath, respectively. The multipath delayed less than $T_c(1+\frac{d}{2})$ distorts the correlation function of direct signal. Because the chip width is inversely proportional to the chipping rate, the higher the chipping rate is, the smaller the range of multipath delays that cause a ranging error is induced. In the case of BOC signals, the higher the subcarrier frequency is, the lower the standard deviation (1-sigma) of multipath error is induced. Meanwhile, when having the same subcarrier frequency and chipping rate, the BOC_{cos} has a better multipath error performance than the BOC_{sin}.

The RMS bandwidth is inversely proportional to the thermal noise jitter of the DLL, so the greater the RMS bandwidth is, the better the code tracking accuracy is introduced. Fig. 4c shows the RMS bandwidth with respect to the receiver bandwidth. As shown in Eq. (15), the RMS bandwidth is greater as more signal power is allocated to frequency components that are further away from the center frequency. When the receiver bandwidth is large enough (i.e., B_r is 24 MHz) for all scenarios, the $BOC_{cos}(2,1)$ has the widest RMS bandwidth for the same reason as spectral efficiency. Meanwhile, the RNSS receiver for civilian uses has a narrow bandwidth for reasons such as implementation cost. Therefore, it is also necessary to analyze the RMS bandwidth in the narrow bandwidth. When the receiver bandwidth is narrow with respect to the

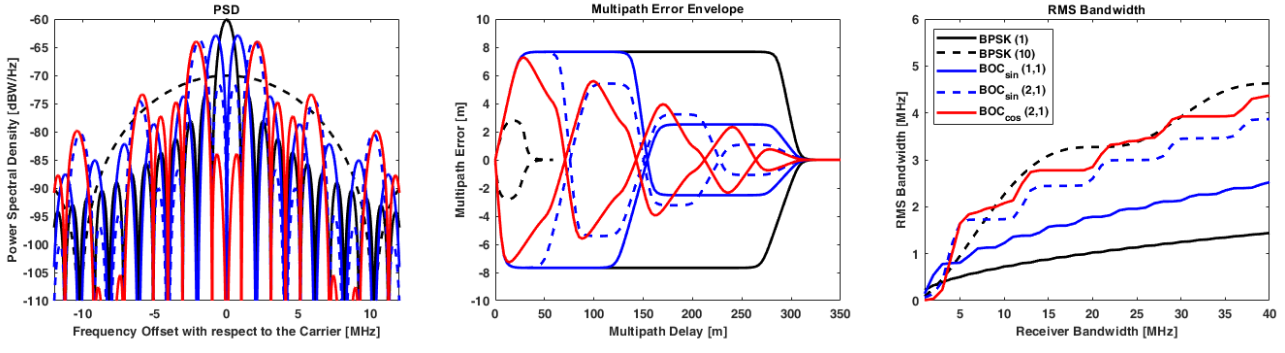

(a) (b) (c)

Fig. 4. FoMs analysis - (a) PSD and spectral efficiency (b) multipath error (c) RMS bandwidth.

Table 3. Simulation results – spectral efficiency, multipath error, and RMS bandwidth.

Scenarios	Spectral efficiency	Max. multipath error [m]	1σ multipath error [m]	Acceptable multipath delay [m]	RMS bandwidth (B_r = 2 MHz) [MHz]	RMS bandwidth (B_r = 24 MHz) [MHz]
BPSK(1)	0.986	7.672	3.725	> 293.052	0.326	1.123
BPSK(10)	0.852	2.781	1.146	> 29.305	0.254	3.325
$BOC_{sin}(1,1)$	0.957	7.672	3.555	> 293.052	0.548	1.957
$BOC_{sin}(2,1)$	0.900	7.665	2.911	> 293.052	0.150	2.995
$BOC_{cos}(2,1)$	0.871	7.270	2.376	> 293.052	0.039	3.393

signal, the RMS bandwidth is determined according to the signal power distribution in the corresponding bandwidth. Table 3 shows that the $BOC_{sin}(1,1)$ has the largest RMS bandwidth when it has a 2 MHz narrow bandwidth.

Table 4. Simulation parameters for trade-off analysis – user received power and UERE.

Scenarios (Center Freq. [MHz])	Tx. power [dBW]	Modulation	Correlator spacing [chips]	Discriminator type	MDR [dB]	DLL filter BW [Hz]	Coherent integration time [ms]
1575.42 2492.028 5019.861	17	BPSK (1)	0.1	Noncoherent EML	-3	2	1

Table 5. Simulation results – user received power and UERE.

Scenarios (Center Freq. [MHz])	User received power @ $el = 30$ [dBW]	Effective C/N_0 @ $el = 30$ [dB-Hz]	1σ DLL jitter @ effective C/N_0 [m]	Ionospheric delay @ $el = 30$[m]	UERE @ $el = 30$ & effective C/N_0[m]
1575.42	-151.160	50.730	0.218	14.358	14.859
2492.028	-155.223	46.667	0.347	5.738	6.903
5019.861	-161.873	40.017	0.807	1.414	4.152

All of these means that the spectral efficiency, the multipath error, and the RMS bandwidth has trade-offs due to the chipping rate and the modulation. When we design a new RNSS signal to be transmitted in congested or narrow frequency bands for civil uses, it is better to select a low chipping rate and the BPSK modulation as signal design parameters. However, this scenario may have a relatively high multipath error and the thermal noise DLL jitter, which will lead to high pseudorange errors.

4.2 User Received Signal Power vs UERE

The user received power and the UERE are related to the center frequency. The RNSS signal with a high center frequency suffers from the high free space loss and atmospheric loss, so it has a low received signal power at the receiving antenna input compared to the signal with a same transmit power and a lower center frequency. The low received signal power makes that the signal has a low effective C/N_0 at the receiver which degrades

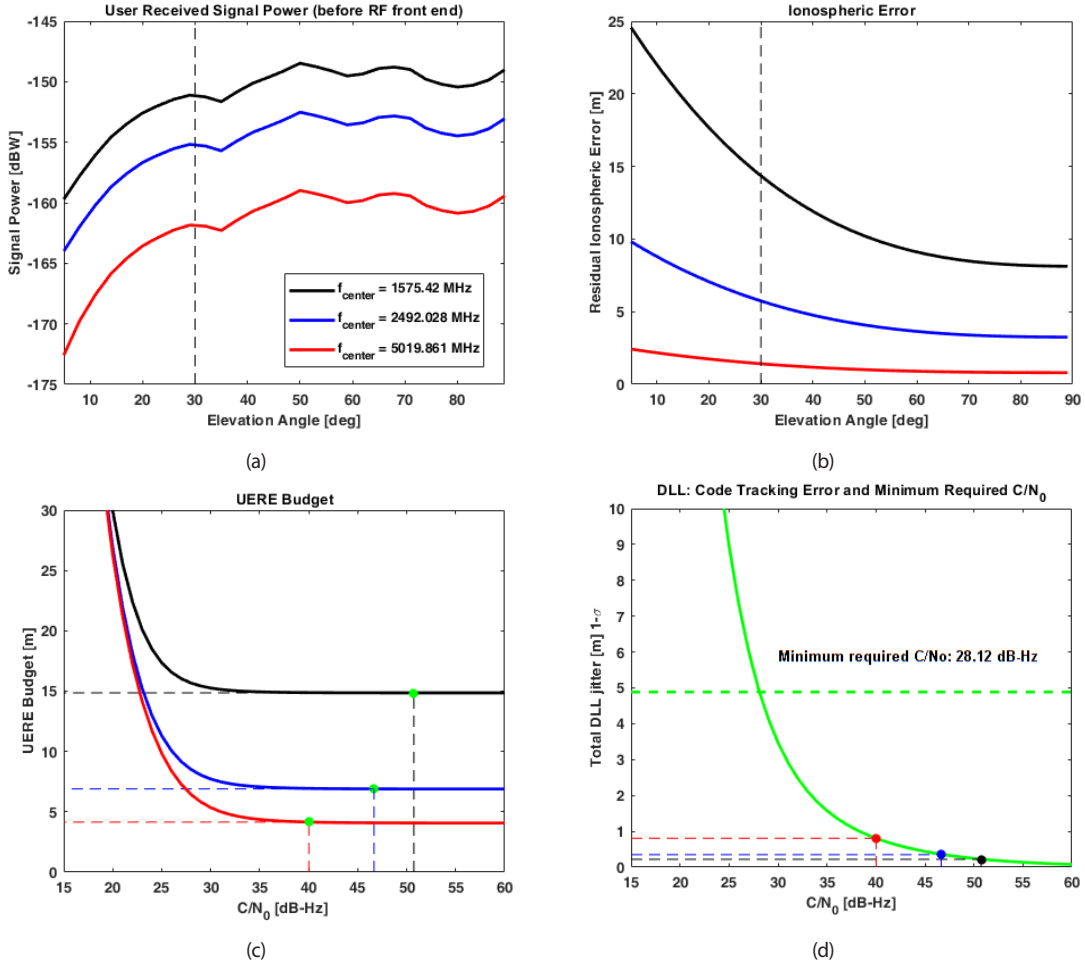

Fig. 5. FoMs analysis - (a) user received power (b) ionospheric error (c) DLL jitter (d) UERE.

the FoMs related to the receiver such as the acquisition probability, the tracking stability, the data demodulation performance, and so on. On the other hand, since the ionospheric delay is inversely proportional to the square of the center frequency, a higher center frequency guarantees a smaller ionospheric delay.

Table 4 represents simulation parameters having a great influence on the two FoMs other than the center frequency. To analyze the trade-offs between the user received signal power and the UERE according to the center frequency, these simulation parameters are common to all scenarios.

Fig. 5 and Table 5 shows the simulation results of the user received power (Fig. 5a), the ionospheric error (Fig. 5b), the DLL jitter (Fig. 5c), and the UERE (Fig. 5d) of all scenarios with the parameters as in Table 4. As we can see in Fig. 5a, the receiving antenna has a gain pattern varying with the elevation angle, the center frequency, and the user received power. Fig. 5b shows that the lower the center frequency is, the smaller the ionospheric error is induced. Meanwhile, the three different center frequencies causes different user received powers from the same transmit power. Fig. 4c shows that the higher the center frequency is, the lower the effective C/N_0 is induced, thereby having the larger DLL jitter. As described before, the UERE is defined as RSS of the URE and the UEE, and the ionospheric delay and the DLL jitter are the components of the UEE. Meanwhile, the ionospheric delay is a dominant component of the UEE (NAVSTAR GPS 1996), the UERE is more affected by the ionospheric delay than the DLL jitter. Therefore, the higher the center frequency is, the better the UERE is expected.

All of these mean that the user received power and the UERE have a trade-off due to the center frequency. When designing a new RNSS signal with a higher center frequency such as S or C band, the transmit power should be higher than that of the L band to provide the same level of the effective C/N_0 to the users on ground. However, it should be noted that the high transmit power shortens the lifetime of the satellite.

5. CONCLUSION

In this paper, we reviewed various FoMs of the RNSS signal performance, then performed trade-off analysis in terms of the several FoMs with respect to the signal design parameters. When designing a new RNSS signal, the signal performance analysis should be performed simultaneously with the selection of the signal candidates. The FoMs described in this paper can be used in the quantitative analysis of the signal performance for a new RNSS signal design. However, the FoMs have trade-offs according to the signal design parameters. Therefore, this paper introduced examples of simulation-based trade-off analysis applicable to next generation RNSS signal design, where the trade-off analysis was performed, for examples, in terms of the spectral efficiency, the multipath error, and the RMS bandwidth according to the chipping rate and the modulation. This confirmed that while BPSK modulated signal with a low chipping rate has better performance in the spectral efficiency, the performance of the multipath error and the tracking accuracy can be poor. The second example considers the trade-off between the user received power and the UERE according to the center frequency. As a result of the analysis, the higher center frequencies have disadvantages in terms of the user received power, but its UERE can be improved.

In conclusion, the FoMs reviewed in this paper can be used as performance indexes of next generation RNSS signals, and it is expected that trade-off analysis using the analysis simulator based on the relationship between these FoMs and signal design parameters can be used to select new RNSS signal candidates.

ACKNOWLEDGMENTS

This research was supported by the Space Core Technology Development Program of the National Research Foundation (NRF) funded by the Ministry of Science & ICT, S. Korea (NRF-2017M1A3A3A02016715).

AUTHOR CONTRIBUTIONS

Han, K. and Won, J. -H. contributed to the design and implementation of the research, to the analysis of the results and to the writing of the manuscript. Conceptualization, Han, K. and Won, J. -H.; methodology, Han, K. and Won, J. -H.; software, Han, K.; validation, Han, K. and Won, J. -H.; formal analysis, Han, K.; investigation, Han, K.; resources, Han, K. and Won, J. -H.; data curation, Han, K.; writing—original draft preparation, Han, K.; writing—review and editing, Han, K. and Won, J. -H.; visualization, Han, K.; supervision, Won, J. -H.; project administration, Won, J. -H.; funding acquisition, Won, J. -H..

CONFLICTS OF INTEREST

The authors declare no conflict of interest.

REFERENCES

Anghileri, M., Paonni, M., Wallner, S., Ávila-Rodríguez, J.-A., & Eissfeller, B. 2008, Estimating the time-to-first-fix for GNSS signals theory and simulation results, European Navigation Conference (ENCGNSS)-Proceedings, Toulouse, France, pp.23-25.

Betz, J. W. 1999, The Offset Carrier Modulation for GPS Modernization, Proceedings of ION 1999, January 25-27, 1999, San Diego, CA, pp.639-648.

Betz, J. W. 2001, Effect of Partial-Band Interference on Receiver Estimation of C/N_0: Theory, Proceedings of ION NTM 2001, Jan. 22-24, 2001, Long Beach, CA, pp.817-828.

Betz, J. W. & Goldstein, D. B. 2002, Candidate Designs for an Additional Civil Signal in GPS Spectral Bands, in Proceeding of The Institute of Navigation National Technical Meeting, San Diego, CA, 28-30 Jan 2002, pp.622-631.

Conley, R., Cosentino, R., Hegarty, C. J., Kaplan, E. D., Leva, J. L., et al. 2006, Performance of Stand-Alone GPS, Chapter 7 in Kaplan, E. D. & Hegarty, C. J. (eds), Understanding GPS: Principles and Applications. 2nd ed. (Boston: Artech House Inc.)

Esper, M., Chao, E. L., & Wolf, C. F. 2020, 2019 Federal Radionavigation Plan (No. DOT-VNTSC-OST-R-15-01), United States. Dept. of Defense

Fine, P. & Wilson, W. 1999, Tracking Algorithm for GPS Offset Carrier Signals, Proceeding of ION 1999, January 25-27, 1999, San Diego, CA, pp.671-676.

Foucras, M., Ekambi, B., Bacard, F., Julien, O., & Macabiau, C. 2014, Optimal GNSS acquisition parameters when considering bit transitions, 2014 IEEE/ION Position, Location and Navigation Symposium-PLANS 2014, 5-8 May 2014, Monterey, CA, USA, pp.804-817. https://doi.org/10.1109/PLANS.2014.6851445

Han, K. & Won, J.-H. 2018, Investigation on the Relationship between GNSS Signal Design Parameters and its Navigation Performance for the Next Generation GNSS Signal Design, Proceedings of the 31st International Technical Meeting of the Satellite Division of The Institute of Navigation (ION GNSS+ 2018), September 24-28, 2018, Miami, Florida, pp.868-875. https://doi.org/10.33012/2018.15887

Han, K. & Won, J.-H. 2019, Development of MATLAB-based Signal Performance Analysis Software for New RNSS Signal Design, Journal of Positioning, Navigation, and Timing, 8, 139-152. https://doi.org/10.11003/JPNT.2019.8.4.139

Hegarty, C. J. 2011, Analytical Model for GNSS Receiver Implementation Losses, Navigation: Journal of The Institute of Navigation, 58, 29-44. https://doi.org/10.1002/j.2161-4296.2011.tb01790.x

Holmes, J. K. & Raghavan, S. 2009, The mean cycle slip time for first-, second-, and third-order PLLs, 2009 IEEE Transactions on Aerospace and Electronic Systems, 7-14 March 2009, Big Sky, MT, USA, pp.1-8. https://doi.org/10.1109/AERO.2009.4839416

Hoque, M. M. & Jakowski, N. 2012, Ionospheric Propagation Effects on GNSS Signals and New Correction Approaches, Chapter 16 in Jin, S. (ed), Global Navigation Satellite Systems-Signal, Theory and Applications (Rijeka, Croatia: InTech)

ITU 2015, Recommendation ITU-R SM.1541-6, Unwanted emissions in the out-of-band domain, International Telecommunication Union.

ITU 2016a, Radio Regulations, Vol. 1, International Telecommunication Union.

ITU 2016b, Radio Regulations, Vol. 3, International Telecommunication Union.

Klobuchar, J. A. 1996, Ionospheric Effects on GPS, Chapter 12 in Parkinson, B. W. & Spilker Jr., J. J. (eds), Global Positioning System: Theory and applications, Volume I (Washington, D.C.: AIAA)

Liu, W., Li, S., Liu, L., Niu, M., & Zhan, X. 2010 A Comprehensive Methodology for Assessing Radio Frequency Compatibility for GPS, Galileo and Compass, Proceedings of the 23rd International Technical Meeting of the Satellite Division of The Institute of Navigation (ION GNSS 2010), Portland, OR, September 21-24 2010, pp.943-954.

Matas, A. 2018, ITU Radio Regulation & Space Traffic Management, 4th Annual Space Traffic Management Conference Embry-Riddle Aeronautical University's College of Aviation 15-19 January 2018, Daytona Beach, Florida USA. https://commons.erau.edu/stm/2018/presentations/18

Misra, P. & Enge, P. 2012, Global Positioning System: signals, measurements and performance, Revised 2nd ed. (Lincoln MA: Ganga-Jamuna Press.)

NAVSTAR GPS User Equipment Introduction 1996, Public Release Version, DOD Joint Program Office, September 1996.

Park, J. U. & Heo, M. B. 2019, Korea PNT Update, 59th Meeting of the Civil GPS Service Interface Committee, Miami, Florida, 16-17 Sep 2019

Rebeyrol, E., Macabiau, C., Julien, O., Ries, L., Issler, J. L., et al. 2006, Signal distortions at GNSS payload level, In: Proceedings od ION GNSS 2006, Institute of Navigation, Fort Worth, Texas, USA, September 26-29 2006, Fort

Worth, TX, pp.1595-1605

Shin, H., Han, K., & Won, J.-H. 2019, Development of End-to-end Numerical Simulator for Next Generation GNSS Signal Design, Journal of Positioning, Navigation, and Timing, 8, 153-164. https://doi.org/10.11003/JPNT.2019.8.4.153

Spilker Jr, J. J. 1996a, GPS Signal Structure and Theoretical Performance, Chapter 3 in Parkinson, B. W. & Spilker Jr., J. J. (eds), Global Positioning System: Theory and applications, Volume I (Washington, D.C.: AIAA)

Spilker Jr, J. J. 1996b, Tropospheric Effects on GPS, Chapter 13 in Parkinson, B. W. & Spilker Jr., J. J. (eds), Global Positioning System: Theory and applications, Volume I (Washington, D.C.: AIAA)

Wallner, S., Avila-Rodriguez, J.-A., & Hein, G. W. 2011, Codes: The PRN Family Grows Again, Inside GNSS, September/October 2011, pp.83-92. https://insidegnss.com/codes-the-prn-family-grows-again/

Ward, P. W. & Betz, J. W. 2006a, Satellite Signal Acquisition, Tracking, and Data Demodulation, Chapter 5 in Kaplan, E. D. & Hegarty, C. J. (eds), Understanding GPS: Principles and Applications. 2nd ed. (Boston: Artech House Inc.)

Ward, P. W. & Betz, J. W. 2006b, Interference, Multipath, and Scintillation, Chapter 6 in Kaplan, E. D. & Hegarty, C. J. (eds), Understanding GPS: Principles and Applications. 2nd ed. (Boston: Artech House Inc.)

Weill, L. R. & Petovello, M. G. 2011, GNSS Solutions: Differences Between Signal Acquisition and Tracking, Inside GNSS, January/February 2011, pp.22-27. https://insidegnss.com/differences-between-signal-acquisition-and-tracking/

Won, J.-H., Eissfeller, B., Schmitz-Peiffer, A., & Colzi, E. 2008, C-Band User Terminal Tracking Loop Stability Analysis for European GNSS Evolution Programme, Proceedings of the 21st International Technical Meeting of the Satellite Division of The Institute of Navigation (ION GNSS 2008), Savannah, GA, September 16-19 2008, pp.1706-1718.

Won, J.-H., Paonni, M., Fontanella, D., & Eissfeller, B. 2011, Receiver Performance Analysis of Advanced Signal-In-Space Modulation Techniques for Next Generation GNSS, Proceedings of the 18th GNSS Workshop, Jeju, S. Korea, 3-4 Nov. 2011.

Xue, R., Sun, Y., & Zhao, D. 2015, CPM signals for satellite navigation in the S and C bands, Sensors, 15, 13184-13200. https://doi.org/10.3390/s150613184

Kahee Han is a Ph. D. student of the Autonomous Navigation Laboratory at Inha University, South Korea. She received B.S. and M.S. degrees from the same university in 2017 and 2019. Her research interests are GNSS signal design and software receiver.

Jong-Hoon Won received the Ph.D. degree in the Department of Control Engineering from Ajou University, Korea, in 2005. After then, he had worked with the Institute of Space Application at University Federal Armed Forces (UFAF) Munich, Germany. He was nominated as Head of GNSS Laboratory in 2011 at the same institute, and involved in lectures on advanced receiver technology at Technical University of Munich (TUM) since 2009. He is currently an associate professor of the Department of Electrical Engineering at Inha University. His research interests include GNSS signal design, receiver, navigation, target tracking systems and self-driving cars.